

## Supporting Information

### **Guanine-derived carbon nanosheets encapsulated Ni nanoparticles for efficient CO<sub>2</sub> electroreduction**

Ying Peng,<sup>a</sup> Shuo Chen,<sup>a</sup> Zhengli Hu,<sup>a</sup> Mengqi Yin,<sup>a</sup> Lishun Pei,<sup>a</sup> Qiaohua Wei<sup>\*a</sup> and Zailai Xie<sup>\*a</sup>

<sup>a</sup> Key Laboratory of Advanced Carbon-Based Functional Materials (Fujian Province University), Fuzhou University, Fuzhou 350016, Fujian, China.

Address correspondence, qhw76@fzu.edu.cn; zlxie@fzu.edu.cn

## Supplementary Figures

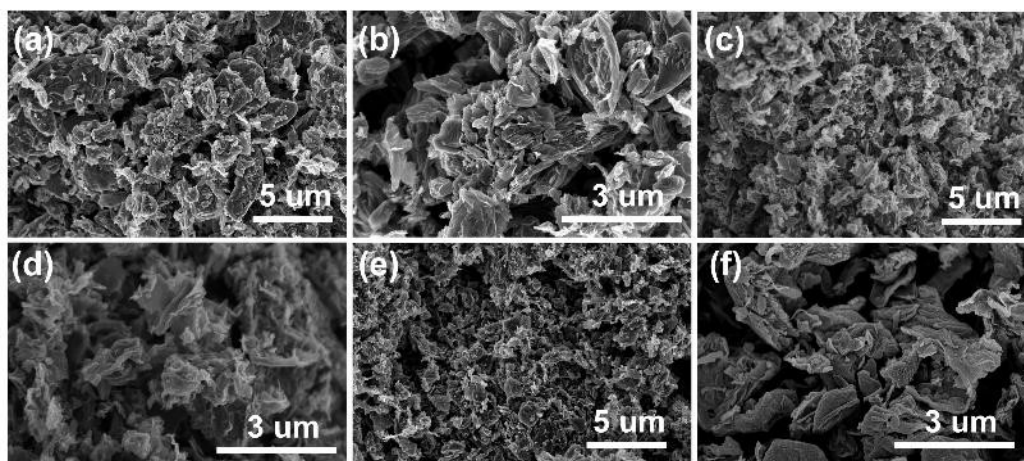


**Fig. S1.** SEM images of (a,b) Ni@NC-900, (c,d) Ni@NC-1100 and (e,f) NC-1000.

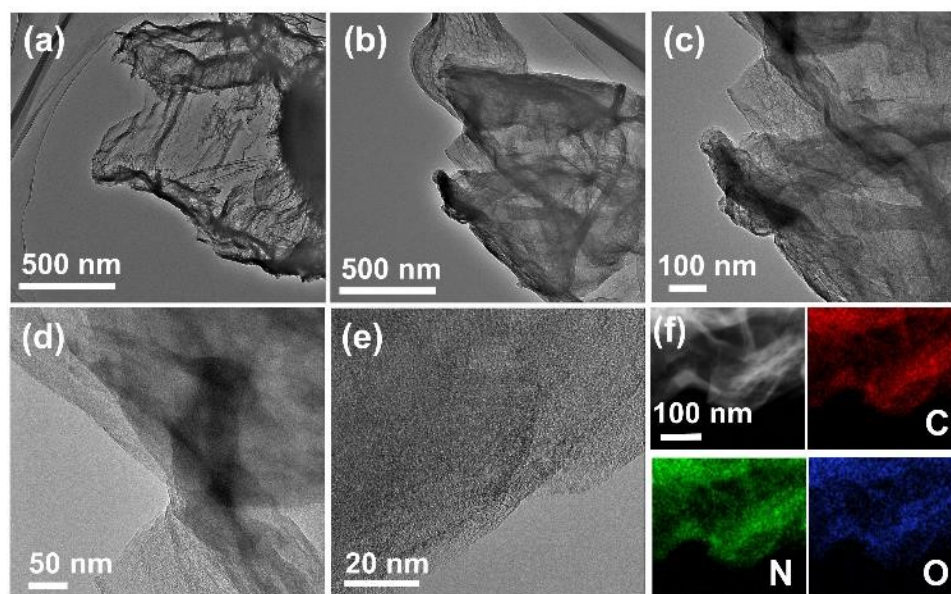


**Fig. S2.** TEM images of NC-1000.

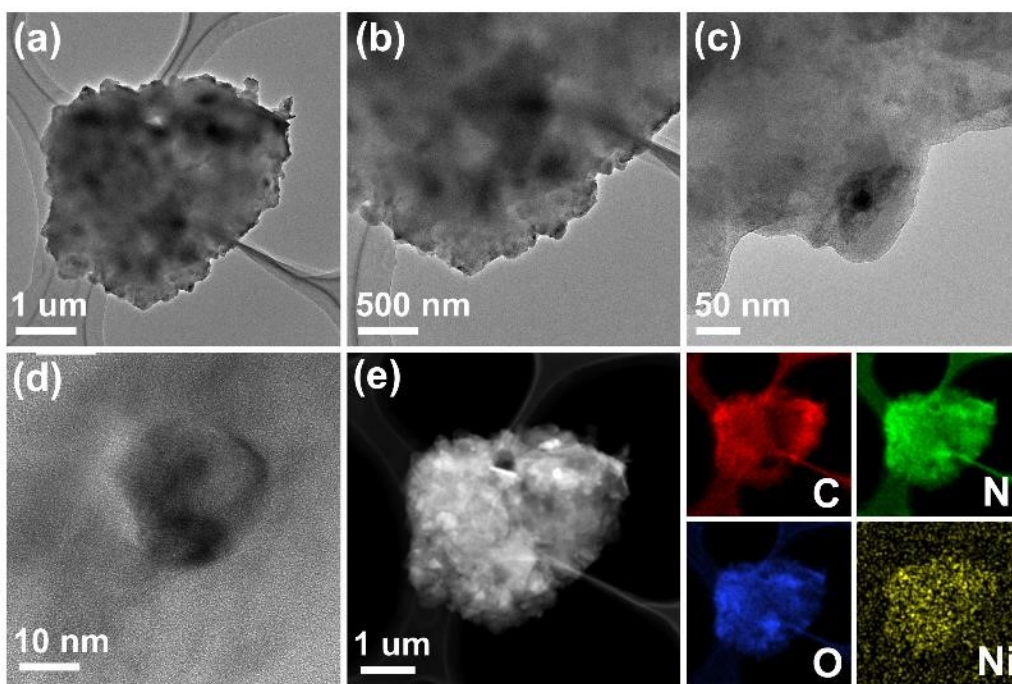


**Fig. S3.** TEM images of Ni@NC-900.

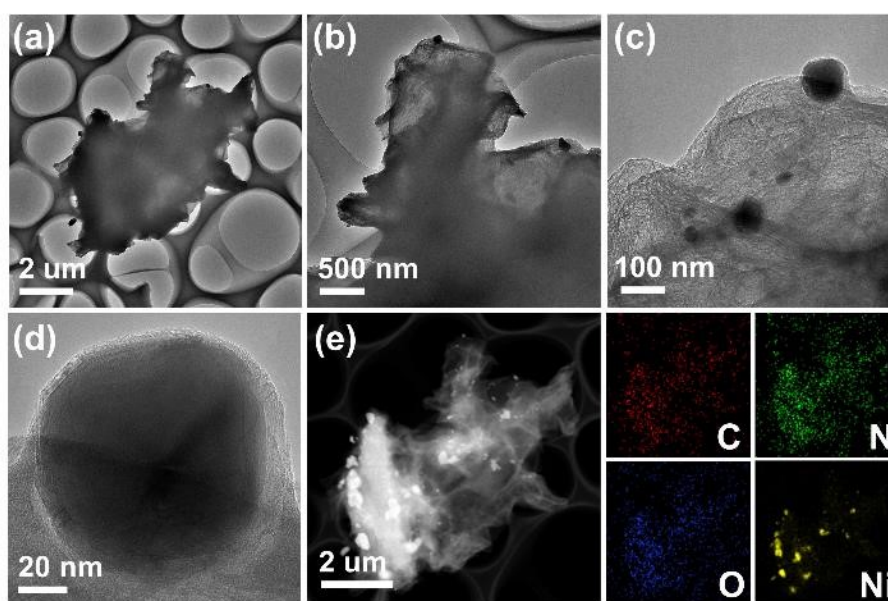


**Fig. S4.** TEM images of Ni@NC-1100.

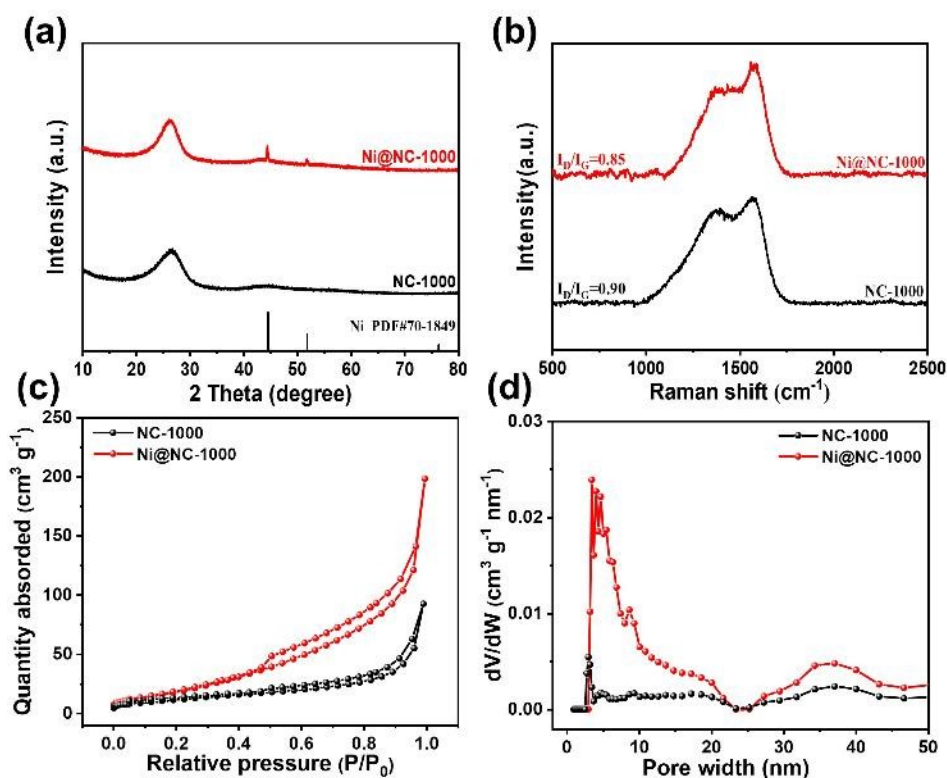


Fig. S5. (a) XRD spectra. (b) Raman spectra. (c)  $N_2$  adsorption-desorption isotherms. (d) Pore size distribution obtained by the BJH method of Ni@NC-1000 and NC-1000.

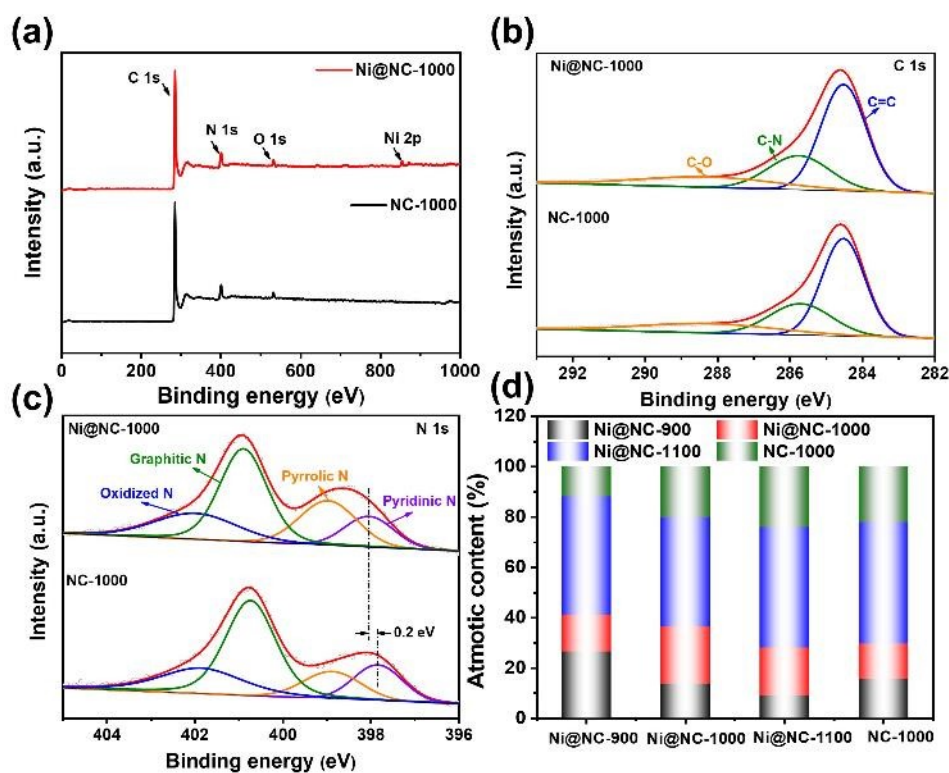
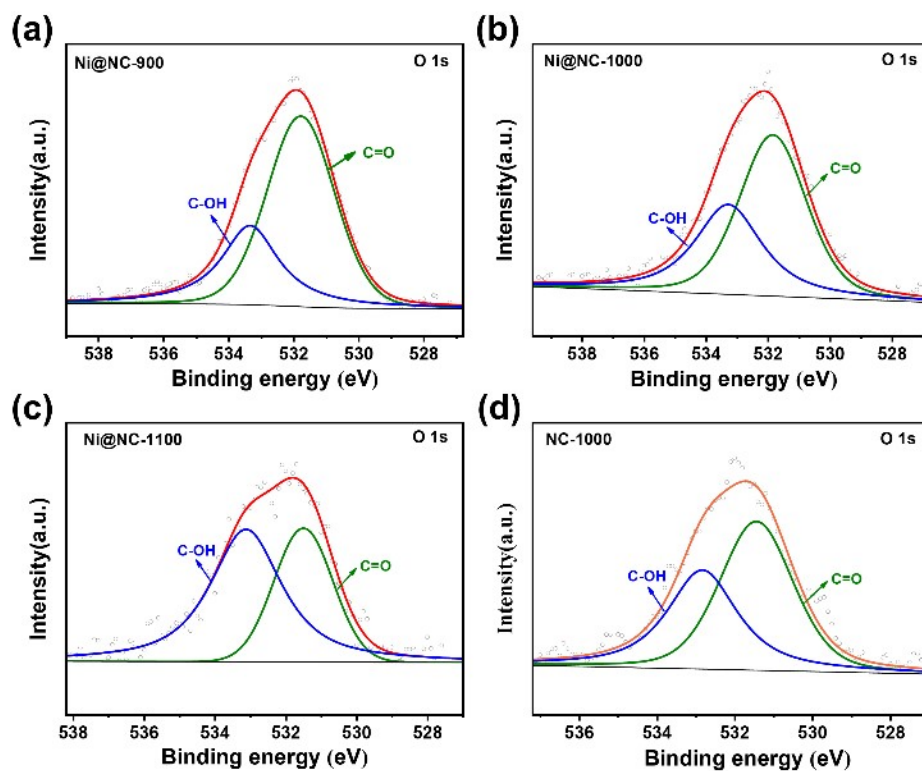
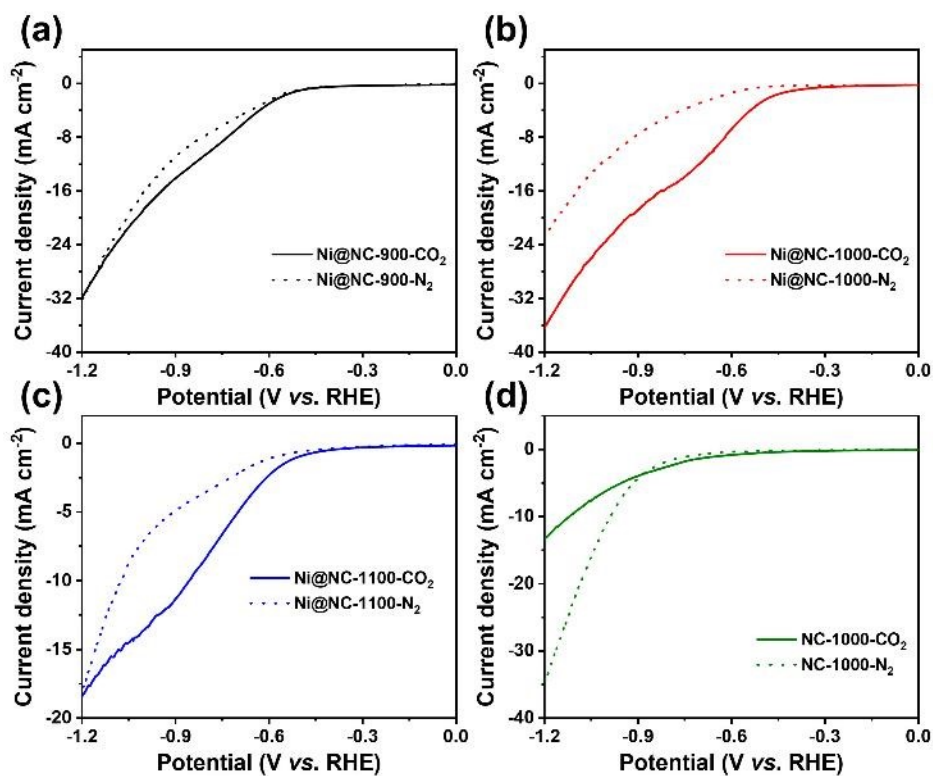


Fig. S6. (a) XPS survey spectra. (b) High-resolution C 1s XPS spectra. (c) High-resolution N 1s XPS spectra. (d) The relative contents of different-type N species in various catalysts.





**Fig. S7.** High-resolution O 1s XPS spectra of (a) Ni@NC-900, (b) Ni@NC-1000, (c) Ni@NC-1100, (d) NC-1000.



**Fig. S8.** LSV curves of (a) Ni@NC-900, (b) Ni@NC-1000, (c) Ni@NC-1100 and (d) NC-1000 in N<sub>2</sub>/CO<sub>2</sub>-saturated 0.5 M NaHCO<sub>3</sub>.

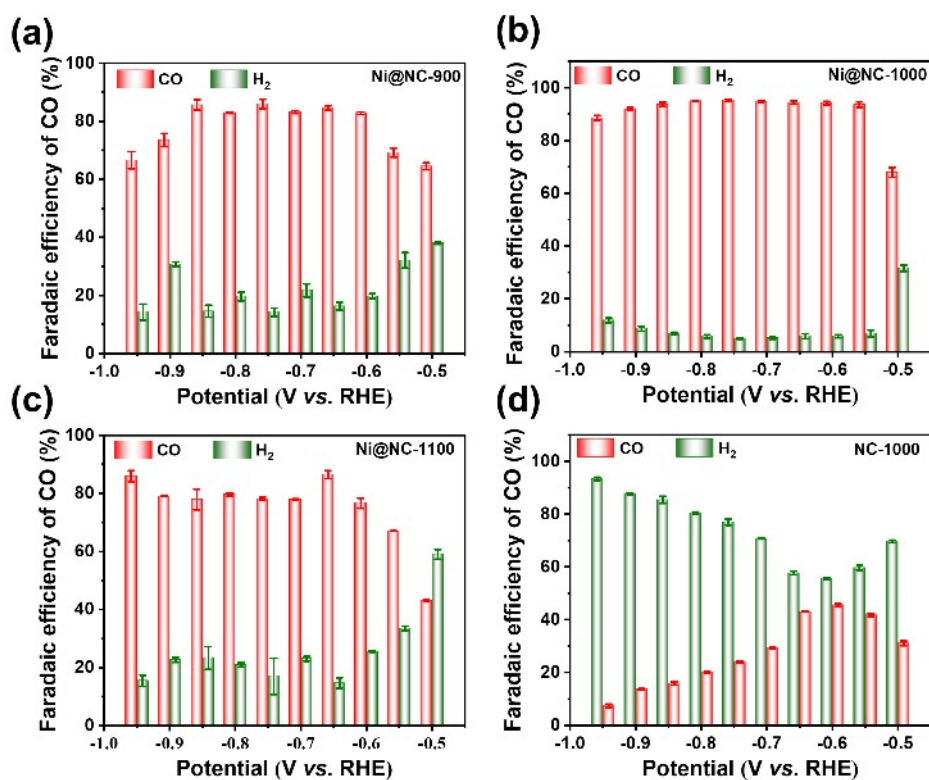


**Fig. S9.** FE<sub>CO</sub> and FE<sub>H<sub>2</sub></sub> of (a) Ni@NC-900, (b) Ni@NC-1000, (c) Ni@NC-1100, (d) NC-1000 at different applied potentials in CO<sub>2</sub>-saturated 0.5 M NaHCO<sub>3</sub>.

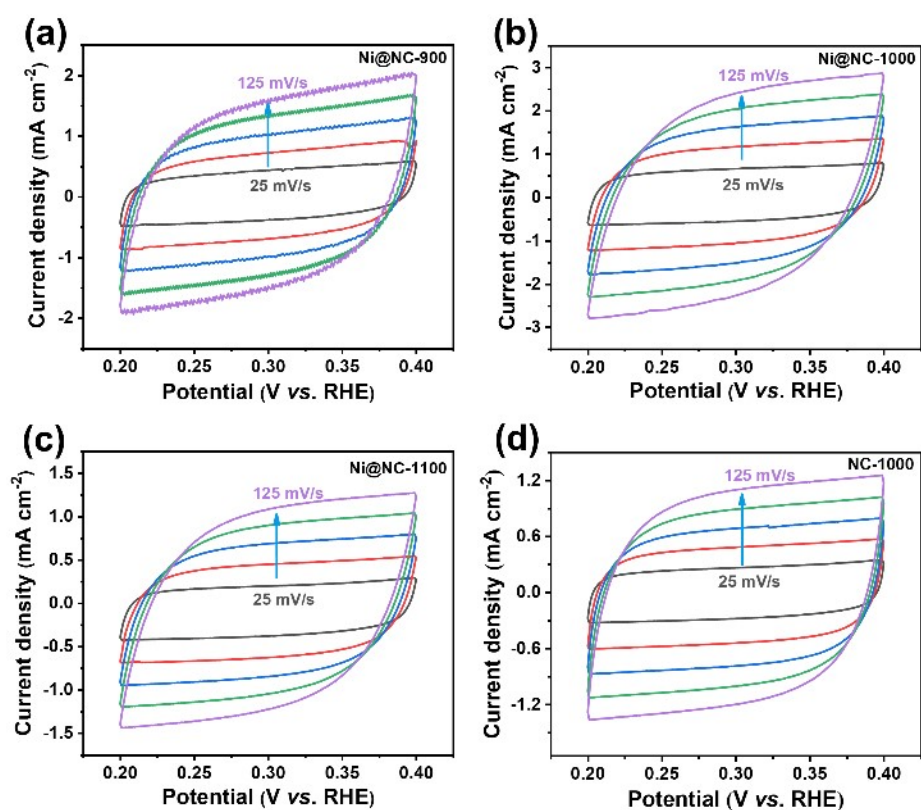


**Fig. S10.** Cyclic voltammety curves of (a) Ni@NC-900, (b) Ni@NC-1000, (c) Ni@NC-1100, (d) NC-1000 in 0.5 M CO<sub>2</sub>-saturated NaHCO<sub>3</sub> solution.

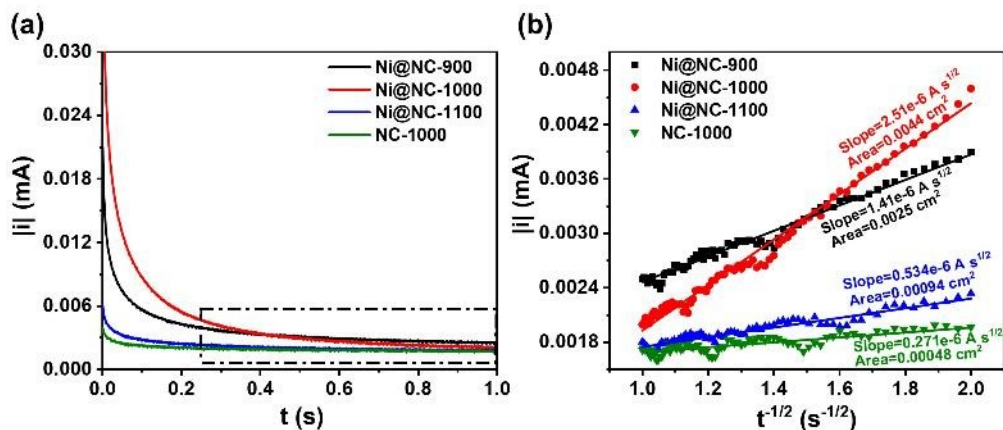


**Fig. S11.** (a) Chronoamperometric response recorded in 0.1 M KCl (containing 5 mM  $\text{K}_3\text{Fe}(\text{CN})_6$ ) after stepping the potential from 0.8 to 0.1 V vs. Ag/AgCl over Ni@NC-X and NC-1000. (b) Linearized plot based on the Cottrell equation for Ni@NC-X and NC-1000 (The first 250 ms were omitted because of double layer charging effects)

The ECSAs of all samples were obtained using the Cottrell equation based on the literature.<sup>1, 2</sup> The Cottrell equation is as follows:

$$i = \frac{nFAC\sqrt{D}}{\sqrt{\pi t}}$$

where  $i$  is the current,  $n = 1$ ,  $D = 4.34 \times 10^{-6} \text{ cm}^2 \text{ s}^{-1}$ ,  $F = 96485 \text{ C mol}^{-1}$ ,  $A$  is ECSA, and  $C$  is the concentration of  $\text{K}_3\text{Fe}(\text{CN})_6$  (5 mM).

The specific testing method is as follows: Firstly, We applied the potential from 0.8 to 0.1 V (vs. Ag/AgCl) in 0.1 M KCl (containing 5 mM  $\text{K}_3\text{Fe}(\text{CN})_6$ ) purged with  $\text{N}_2$  and recorded the chronoamperometric response within 1 s, as shown in Fig. R8 (a). Then we plotted a graph of  $i$  and  $t^{-1/2}$  and fit it to obtain the slope, as shown in Fig. R8 (b). The ECSAs of all catalysts can be calculated by slope. According to the results, the ECSAs of Ni@NC-900, Ni@NC-1000, Ni@NC-1100 and NC-1000 were assessed to be 0.0025, 0.0044, 0.00094 and 0.00048 cm $^2$ , respectively.

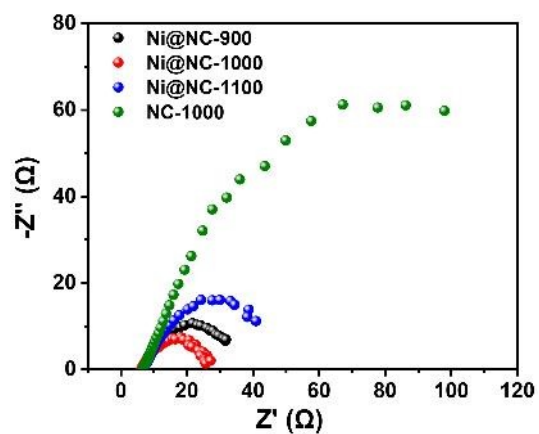


**Fig. S12.** The EIS plots of Ni@NC-X and its comparison sample NC-1000.

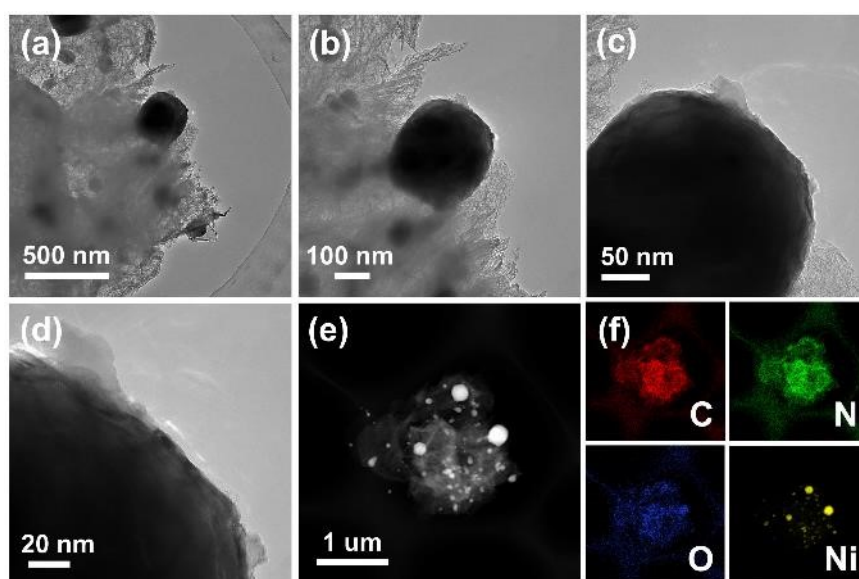


**Fig. S13.** TEM images of spent Ni@NC-1000.



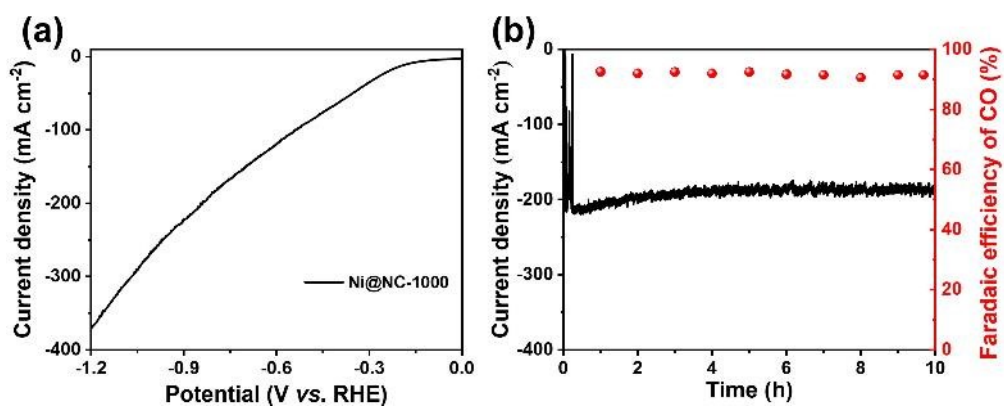


Fig. S14. Flow cell measurement of Ni@NC-1000 at -0.9 V (vs. RHE) in 1 M KOH.

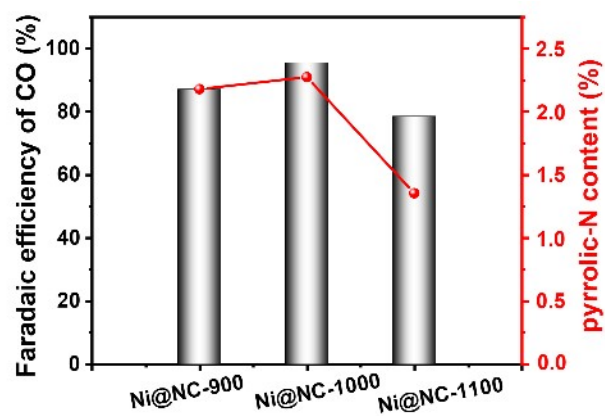


Fig. S15. The relationship between the content of pyrrolic N in catalysts and the corresponding CO<sub>2</sub>RR activity.

## Supplementary Tables

**Table S1.** Summary of BET results for Ni@NC-X and NC-1000 catalysts.

Catalyst	BET Surface Area (m <sup>2</sup> /g)	Adsorption Pore Diameter (nm)	Pore Volume (cm <sup>3</sup> /g)
<b>Ni@NC-900</b>	63	9.9	0.16
<b>Ni@NC-1000</b>	77	10.1	0.31
<b>Ni@NC-1100</b>	65	10.2	0.18
<b>NC-1000</b>	44	12.1	0.14

**Table S2.** The contents of carbon, nitrogen, oxygen and nickel elements in various catalysts.

Catalyst	C wt%	N wt%	O wt%	Ni wt%
<b>Ni@NC-900</b>	81.88	14.17	3.45	0.5
<b>Ni@NC-1000</b>	87.66	9.41	2.38	0.56
<b>Ni@NC-1100</b>	90.95	6.7	1.75	0.6
<b>NC-1000</b>	88.54	8.71	2.5	-

**Table S3.** The relative contents of four major N species in various catalysts.

N Species Catalyst	Pyridinic N (%)	Pyrrolic N (%)	Graphitic N (%)	Oxidized N (%)
<b>Ni@NC-900</b>	26.5	14.5	47.1	11.9
<b>Ni@NC-1000</b>	13.6	22.8	43.4	20.2
<b>Ni@NC-1100</b>	8.9	19.1	47.8	24.2
<b>NC-1000</b>	15.5	14	48.3	22.2

**Table S4.** Summary of CO<sub>2</sub>RR performance from recent literature

Catalyst	Electrolyte	FE <sub>CO</sub> (%)	Potential (V vs. RHE)	j <sub>CO</sub> (mA cm <sup>-2</sup> )	Ref
<b>Ni@NC-1000</b>	0.5 M NaHCO <sub>3</sub>	95.6	-0.75	12.3	This work
<b>Ni-NCN</b>	0.5 M KHCO <sub>3</sub>	96.6	-0.83	9.8	3
<b>Ni-SAC@NC</b>	0.5 M KHCO <sub>3</sub>	95.0	-0.6	5.7	4
<b>NiSA@N<sub>3</sub>-C</b>	0.5 M KHCO <sub>3</sub>	96	-0.83	18.87	5
<b>Ni-NC/NHCSs-600</b>	0.5 M NaHCO <sub>3</sub>	98.57	-0.87	14.2	6
<b>Ni@N-C</b>	0.5 M KHCO <sub>3</sub>	90	-0.8	17	7
<b>Ni@N-C/rGO 4,4'-bipy</b>	0.5 M KHCO <sub>3</sub>	88	-0.97	20	8
<b>Ni-NC(HPU)</b>	0.5 M KHCO <sub>3</sub>	91	-0.8	24.7	9
<b>SA-NiNG-NV</b>	0.5 M KHCO <sub>3</sub>	96	-0.7	10	10
<b>NC-CNTs (Ni)</b>	0.1 M KHCO <sub>3</sub>	90	-0.8	7.5	11
<b>Ni, N-C-800</b>	0.1 M KHCO <sub>3</sub>	94.8	-0.86	18.2	12
<b>Ni-N-C-NH<sub>4</sub>Cl</b>	0.5 M KHCO <sub>3</sub>	98	-0.62	8.5	13
<b>Ni SAs</b>	0.5 M KHCO <sub>3</sub>	97	-0.8	6.8	14

## Reference

- 1 H. Q. Liang, S. Zhao, X. M. Hu, M. Ceccato, T. Skrydstrup and K. Daasbjerg, *ACS Catal.*, 2021, **11**, 958-966.
- 2 Y. C. Zhang, C. S. Cao, X. T. Wu and Q. L. Zhu, *Inorg. Chem. Front.*, 2021, **8**, 2461-2467.
- 3 C. Lv, K. Huang, Y. Fan, J. Xu, C. Lian, H. Jiang, Y. Zhang, C. Ma, W. Qiao, J. Wang and L. Ling, *Nano Energy*, 2023, **11**, 108384.
- 4 Y. Guo, S. Yao, Y. Xue, X. Hu, H. Cui and Z. Zhou, *Appl. Catal., B*, 2022, **304**, 120997.
- 5 L. Qiu, S. Shen, C. Ma, C. Lv, X. Guo, H. Jiang, Z. Liu, W. Qiao, L. Ling and J. Wang, *Chem. Eng. J.*, 2022, **440**, 135956.
- 6 S. Gong, W. Wang, R. Lu, M. Zhu, H. Wang, Y. Zhang, J. Xie, C. Wu, J. Liu, M. Li, S. Shao, G. Zhu and X. Lv, *Appl. Catal., B*, 2022, **318**, 121813.
- 7 F. Wang, G. Wang, P. Deng, Y. Chen, J. Li, D. Wu, Z. Wang, C. Wang, Y. Hua and X. Tian, *Small*, 2023, **19**, 2301128
- 8 F. Wang, Z. Miao, J. Mu, Y. Zhao, M. Liang, J. Meng, X. Wu, P. Zhou, J. Zhao, S. Zhuo and J. Zhou, *Chem. Eng. J.*, 2022, **428**, 131323.
- 9 Y. Li, X. F. Lu, S. Xi, D. Luan, X. Wang and X. W. Lou, *Angew. Chem., Int. Ed.*, 2022, **61**, 2201491
- 10 C. Jia, S. Li, Y. Zhao, R. K. Hocking, W. Ren, X. Chen, Z. Su, W. Yang, Y. Wang, S. Zheng, F. Pan and C. Zhao, *Adv. Funct. Mater.*, 2021, **31**, 2107072.
- 11 Q. Fan, P. F. Hou, C. H. Choi, T. S. Wu, S. Hong, F. Li, Y. L. Soo, P. Kang, Y. S. Jung and Z. Y. Sun, *Adv. Energy Mater.*, 2020, **10**, 190368.
- 12 X. Tan, C. Yu, S. Cui, L. Ni, W. Guo, Z. Wang, J. Chang, Y. Ren, J. Yu, H. Huang and J. Qiu, *Chem. Eng. J.*, 2022, **433**, 131965.
- 13 D. Ping, F. Yi, G. Zhang, S. Wu, S. Fang, K. Hu, B. B. Xu, J. Ren and Z. Guo, *J. Mater. Sci. Technol.*, 2023, **142**, 1-9.
- 14 Z. Li, D. He, X. Yan, S. Dai, S. Younan, Z. Ke, X. Pan, X. Xiao, H. Wu and J. Gu, *Angew. Chem., Int. Ed.*, 2020, **59**, 18572-18577.